International Journal of Coal Geology 123 (2014) 52–61

Contents lists available at ScienceDirect

International Journal of Coal Geology

journal homepage: www.elsevier.com/locate/ijcoalgeo

Multi-component gas transport and adsorption effects during CO_2 injection and enhanced shale gas recovery

Ebrahim Fathi [a,*], I. Yucel Akkutlu [b,1]

[a] West Virginia University, United States
[b] Texas A&M University, United States

ARTICLE INFO

Article history:
Received 16 April 2013
Received in revised form 27 July 2013
Accepted 28 July 2013
Available online 8 August 2013

Keywords:
Shale
Adsorption
Multi-component transport
Recovery
Sequestration

ABSTRACT

A new mathematical model is introduced based on the Maxwell–Stefan formulation to simulate multi-component (CH_4–CO_2) transport in resource shale. The approach considers competitive transport and adsorption effects in the organic (kerogen) micropores of the shale during CO_2 injection and enhanced CH_4 recovery. Following the primary production, injection of CO_2 into organic-rich shale initiates co- and counter-diffusive transport and competitive sorption among the molecules. Consequently, the incoming CO_2 molecules activate and displace the in-place CH_4 molecules. Competitive sorption rates, however, could be controlled by the diffusive mass fluxes during the injection and production operations. Nature of the transport processes should therefore be understood clearly. In this paper, we first show that the widely used single-component Langmuir gas behavior is, in fact, a limiting case of the generalized formulation. The latter, however, includes not only the anticipated binary effects (due to the co-existence of two components with different molecular size and adsorption capacity) but also additional nonlinear effects due to the direction of diffusive mass fluxes and to the lateral interactions of the adsorbed gas molecules in the micropores. Following, we incorporate the multi-component formulation to a shale gas flow model to consider CO_2 injection and enhanced shale gas recovery processes in a single horizontal well setup with multiple fractures. The simulation involves primary gas production for ten years followed by three-stages of operations including injection of CO_2 for five years, a short soaking period, and finally production for 30 years. Dynamics of the production stages is then investigated with varying initial/boundary conditions. It is shown that the counter diffusion and competitive adsorption in the micropores could generate nontrivial effects at the reservoir-scale such that the predicted CH_4 production is significantly enhanced. The investigation is important for our understanding and the design of CO_2 injection and enhanced shale gas recovery processes.

1. Introduction

When subsurface storage of anthropogenic carbon dioxide (CO_2) is considered, among the geological formations, gas shale, much like coalbed methane, keeps a unique place with a distinct gas trapping mechanism: physical adsorption (Kang et al., 2011; Nuttall and Rushing, 2005). Under the subsurface conditions and depending on the thermal maturity of organic materials in the shale, CO_2 sorption capacity of the shale is larger than that for methane (CH_4) especially in the primary (or micro-) pore volume (Busch et al., 2008; Shi and Durucan, 2008). This is a remarkable observation not only for sequestration but also from enhanced shale gas production point of view as it implicitly points out that stronger affinity of CO_2 to the organic materials of shale could initiate an added mechanism of displacement of the originally in-place CH_4, when CO_2 is introduced into the shale gas environment. Thus, CO_2-enhanced shale gas recovery is proposed as an improved natural gas recovery technique.

Although CO_2-enhanced shale gas recovery technique has not been commercialized yet, attempts have been made to study the feasibility of the technique in the Middle and upper Devonian black shales in the Appalachian Basin in West Virginia, Pennsylvania and eastern Kentucky (Boswell, 1996; Schepers et al., 2009). In the United States large production from numerous wells and an extensive pipeline structure associated with organic shale gas reservoirs located near major population centers such as the Barnett, adjacent to Dallas-Fort Worth, and the Marcellus, New York exist. When these resources are depleted, they can be considered as good candidates to store carbon dioxide much like they stored methane both in the adsorbed and free states over geologic time spans.

CO_2 sequestration and enhanced shale gas recovery involve phenomena of fundamental interest in a chemically and structurally intricate porous medium, however. In general, the technique involves three stages: (1) convective/dispersive flow of the gas phase (injected CO_2 and released CH_4 molecules), in particular in the fractures; (2) diffusive/

* Corresponding author at: 345A Mineral Resources Building, College of Engineering and Mineral Resources, Morgantown, WV 26506-6070, United States. Tel.: +1 304 2932449.
E-mail address: ebfathi@mail.wvu.edu (E. Fathi).
[1] Petroleum Engineering Department, 401T Richardson Building, College Station TX 77843-3116, United States. Tel.: +1 979 845 4069.

0166-5162/$ – see front matter © 2013 Elsevier B.V. All rights reserved.
http://dx.doi.org/10.1016/j.coal.2013.07.021

dispersive gas transport in the secondary pore structure of the shale matrix, i.e., fractures and the macro-pores; and (3) multi-component sorption phenomena, in particular in the primary (micro-) pore structure of the shale matrix, e.g., co- and counter diffusion and competitive adsorption. These simultaneously take place in the shale matrix within different characteristic times of mass transport (flow, diffusion and sorption) and characteristic length scales, i.e., the scales of hydraulic fracture stages, of shale matrix and of the internal surface area of the matrix pores. As the consequence of these, the incoming CO_2 molecules are expected to activate and displace the in-place CH_4 molecules in the shale matrix.

Earlier theoretical attempts investigating shale gas production involved numerical simulators developed in the 'spirit' of modeling the naturally fractured conventional gas and coalbed methane reservoirs with single permeability and dual porosity fields (Eccles et al., 2009; Leahy-Dios et al., 2011). Often the gas mass balance appeared in these approaches in terms of a gas quality such as molar density, concentration or pressure, which is averaged over a single-porosity, or uni-pore, matrix. When it is written in one-dimensional space for the concentration of the gas component, the balance for a finite-size matrix typically reads as

$$\varphi\frac{\partial C}{\partial t}+\left(1-\varphi-\varphi_f\right)\frac{\partial C_\mu}{\partial t}=\frac{\partial}{\partial x_1}\left(\varphi D_m\frac{\partial C}{\partial x_1}\right) \tag{1}$$

where φ and φ_f are the constants of matrix and fracture porosity, and C and C_μ are the free and adsorbed gas molar densities, i.e., concentrations, in the matrix block, respectively. Notice that Eq. (1) is another form of Fick's second law written for a fluid adsorbing in porous medium. The adsorbed amount is often accounted for during the calculations using a nonlinear equilibrium adsorption model, such as Langmuir isotherm:

$$C_\mu = C_m b' C/(1+b' C). \tag{2}$$

The presence of a diffusive mass transport with a constant diffusivity, D_m, was assumed next at the matrix–fracture interface and the averaging is performed using a priori parabolic concentration profile across the half-length R of the matrix block (Shi and Durucan, 2005)

$$\varphi\frac{\partial \overline{C}}{\partial t}+\left(1-\varphi-\varphi_f\right)\frac{\partial \overline{C_\mu}}{\partial t}=\frac{3}{R}\varphi D_m\left(\frac{\partial C}{\partial x_1}\right)_{x_1=R} \tag{3}$$

with the block-averaged free and adsorbed gas concentrations are assigned to symbols with an over bar. An inner boundary condition is often imposed dictating that no concentration gradient exists at the center of the matrix block (i.e., $\partial C(0,t)/\partial x_1 = 0$). Consequently, the balance showing the time evolution of the averaged concentration was coupled to the mass balance equation for the fracture network using the diffusive mass exchange term at the matrix–fracture interface as a source/sink term in the latter:

$$\varphi\frac{\partial \overline{C}}{\partial t}+\left(1-\varphi-\varphi_f\right)\frac{\partial \overline{C_\mu}}{\partial t}=\varphi\sigma D_m\left(C_f-\overline{C}\right) \tag{4a}$$

$$\varphi_f\frac{\partial C_f}{\partial t}+\frac{\partial}{\partial x_2}\left(\varphi_f v_f C_f\right)=\varphi_f\sigma D_m\left(\overline{C}-C_f\right). \tag{4b}$$

Here, $\sigma = 15/R^2$ is the coefficient of mass exchange between the matrix and the fracture (i.e., the transfer function). The accompanying gas mass balance, Eq. (4b), dictates that the fractures are the places of transient (Darcian) flow with a corresponding shale matrix permeability field.

When complemented with appropriate reservoir initial and boundary conditions, i.e., closure of the initial/boundary value problem, the formulation may capture certain behavior of gas production in the field. However, it ignores several aspects of the shale gas physics as it significantly reduces the size of the problem. Those are the emphases of this paper since they are important to shale gas production and they may become critical considerations for the design and application of CO_2 sequestration and enhanced shale gas recovery. First, the conventional model assumes that partitioning of the free and the adsorbed gas in the matrix block occurs instantaneously and that the only resistance to the free gas release from the matrix is due to the so-called transfer function, which is essentially an averaged diffusive mass flux at the matrix–fracture interface (Gwo et al., 1998; Sarma, and Aziz, 2006; Warren and Root, 1963). The resistance obviously takes a finite value when the matrix block is surrounded by a network of uniformly distributed dominant single fractures and maintains a finite size, R. In essence, the conventional approach (i) considers the existence of discrete matrix blocks in the reservoir, (ii) treats the gas behavior in the matrices as a molecular diffusion (heat conduction) problem and (iii) controls the gas release from the matrices using the transfer function as a numerical valve. It is, however, true that the shale matrix can be described and characterized suitably using a multi-scale pore structure: the total pore volume of a block is made not only of micro- and macro-pores but also due to a micro-fracture network, which may significantly contribute to gas release during the production. Although the characteristic dimensions of these fractures could be very small relative to the dominant single fractures, they may be considered as the places for convective transport. Thus, their presence in the matrices not only makes the identification and discretization of the blocks difficult, if not impossible, but also changes the nature of gas transport, modifying the traditional matrix problem to a convective–diffusive one (Tinni et al., 2012).

Second, the diffusive nature of the mass transport has to be re-visited for the shale matrices. It is well documented in the literature that bulk diffusion and Knudsen (molecular streaming) flow of the gas molecules are the main mechanisms for the free gas migration in the macro-pores; whereas surface diffusion is the mechanism for the adsorbed molecules through the physically adsorbed layer on the micro-pore walls (Fathi and Akkutlu, 2012, 2013). It is perhaps straightforward to incorporate these mechanisms with the traditional approach using Fick's first law, although the problem becomes a challenging one when multi-component gas behavior is considered. Flow of the injected CO_2 in a complex multi-scale fracture network initiates counter-diffusive and competitive adsorption processes between the CO_2 and CH_4 molecules in the primary pore structure of the shale matrix, modifying the gas transport, in particular, and the nature of the surface diffusion on the adsorption layer. The conventional models (with the mass balances written for each component of the gas), do not consider such steric effects due to multi-component nature of the problem. Although competitive adsorption and multi-component (co- and counter-) diffusion processes are well recognized in the engineering literature (Chen et al., 2010; Ryan et al., 2011; Zhou et al., 2012) and they are considered important for practical reasons (e.g., gas separators), our understanding of the system dynamics is limited due to difficulties of measuring quantities related to transport in the mixture (Yi et al., 2008).

The purpose of this work is to investigate the CO_2 sequestration and enhanced shale gas recovery numerically using a new multi-continuum modeling approach that does not have the above-mentioned matrix-averaging and multi-component transport limitations of the conventional approach. A new formulation is proposed for the shale gas transport using Maxwell–Stefan formulation and for kinetics of gas release from the pores using a linear relationship describing net rate of gas mass interchange between the fractures and the pores. The governing equations consider that the gas transport in organic-rich shales involves a matrix with triple porosity continua (with organic and inorganic pores and fractures) with a serial coupling, each represented by its own flow and transport processes:

- fractures are the places where the injected and released 'free' gas flows (i.e., convective and dispersive transport);
- the inorganic macropores make up the portion of pore volume where convective–diffusive transport takes place for the free gas;

- organic (kerogen) micropores are part of the solid shale material which retains the gas in both adsorbed and free states and allows their pore and surface transport. The resistance in the micropores is due to surface diffusion.

2. Binary gas transport model for CO_2 injection and enhanced shale gas recovery

According to this interpretation the kerogen pore network hydraulically communicates with the inorganic matrix such that mass transport takes place in the following sequence during the gas release: organic → inorganic → fracture. The application of multi-continua requires that each porous medium is distributed continuously in space and holds the porous media conditions specified by Bear and Bachmat (1991). Governing equations describing the gas mass balance in dual-continua are the same as single continuum model; however, they need special considerations for volume consistency and the mass exchange terms. One-dimensional shale gas system consists of the following mass balances for the components 1 (CH_4) and 2 (CO_2).

Free gas mass balance in the organic micropores (kerogen):

$$\frac{\partial\left(\varepsilon_{kp}\phi C_{ki}\right)}{\partial t}+\frac{\partial\left[\varepsilon_{ks}\left(1-\phi-\phi_f\right)C_{\mu i}\right]}{\partial t}=\frac{\partial}{\partial x}\left(\varepsilon_{kp}\phi D_{ki}\frac{\partial C_{ki}}{\partial x}\right)+\frac{\partial}{\partial x}\left(\varepsilon_{ks}\left(1-\phi-\phi_f\right)D_{si}\frac{\partial C_{\mu i}}{\partial x}\right)\quad i=1,2 \tag{5}$$

Here, x–t are the space–time coordinates. $C_{ki}(x,t)$ and $C_{\mu i}(x,t)$ represent the amounts of free gas and adsorbed-phase in kerogen in terms of moles per kerogen pore volume and moles per kerogen solid volume, respectively. In Eq. (5) ϕ and ϕ_f are the total interconnected matrix porosity and fracture porosity in shale, respectively. These are dynamic quantities that may vary significantly in time and space due to void volume compressibility and adsorption layer effects with the changing pore pressure (Kang et al., 2011; Santos and Akkutlu, 2013). ε_{ks} is the total organic content (TOC) in terms of organic grain volume per total grain volume and ε_{kp} is kerogen pore volume per total matrix pore volume. Hence, $\varepsilon_{kp}\phi$ is equal to kerogen porosity ϕ_k and it can be written in terms of the bulk volume, total pore volume and kerogen pore volume as $\phi_k=(V_{kp}/V_p)(V_p/V_b)$. Similarly, $\varepsilon_{ks}(1-\phi-\phi_f)$ is the fractional kerogen solid volume, i.e., $1-\phi_k$, which can be written in terms of volumes as $1-\phi_k=(V_{ks}/V_{ms})(V_{ms}/V_b)$. Here V_{kp} and V_{ks} are the kerogen pore and grain volumes and V_{ms}, V_p and V_b are grain, pore and bulk volumes for the matrix. D_{ki} is the tortuosity-corrected coefficient of molecular diffusion for the free gas in kerogen. Finally, D_{si} is diffusion coefficient related to adsorbed phase transport, i.e., surface transport. The diffusion coefficients are considered in terms of a total mass flux which is, for simplicity in the analysis of the experimental work, taken as Fickian in nature. Note that the subscripts k, m and f refer to quantities related to the kerogen, inorganic matrix and fracture, respectively.

Free gas mass balance in the inorganic matrix (i.e., macropores):

$$\frac{\partial\left[\left(1-\varepsilon_{kp}\right)\phi C_i\right]}{\partial t}=\frac{\partial}{\partial x}\left[\left(1-\varepsilon_{kp}\right)\phi D_i\frac{\partial C_i}{\partial x}\right]+\frac{\partial}{\partial x}\left(\left(1-\varepsilon_{kp}\right)\phi C_i\frac{k_m}{\mu_i}\frac{\partial p_i}{\partial x}\right)-W_{km} \tag{6}$$

where $(1-\varepsilon_{kp})\phi$ is the inorganic porosity ϕ_I. D_i is the tortuosity-corrected coefficient of molecular diffusion, k_m the absolute permeability of the inorganic matrix, and μ_i the dynamic gas viscosity. The mass exchange between two continua is captured by a coupling term W_{km} which is a function of shape factor Ω, diffusive transport Ψ and the concentration difference between the two continua at the interface.

Free gas mass balance in the fracture network:

$$\frac{\partial\left(\phi_f C_{fi}\right)}{\partial t}=\frac{\partial}{\partial X}\left(\phi_f K_L\frac{\partial C_{fi}}{\partial X}\right)+\frac{\partial}{\partial X}\left(C_{fi}\frac{k_f}{\mu_i}\frac{\partial p_{fi}}{\partial X}\right)-W_{mf} \tag{7}$$

which is also convective–dispersive. The mass transfer functions introduced in Eqs. (6) and (7) are defined as

$$W_{kmi}=\Omega_m\Psi_{ki}(C_i-C_{ki}) \tag{8}$$

$$W_{mfi}=\Omega_f\Psi_{mi}\left(C_{fi}-\overline{C}_i\right). \tag{9}$$

These equations can be reduced to a simpler form considering the definitions of ϕ_k and ϕ_I and that the temporal changes in pore volumes are considered negligible (Akkutlu and Fathi, 2012). The thermodynamic behavior of gas can be represented by the compressibility equation of state $p=zCRT$ with a reasonable accuracy, see Fathi and Akkutlu (2009). Furthermore molecular diffusion in the inorganic pores and micro-fractures is small compared to viscous flow and can be ignored (Bear, 1972). Finally, the micro- and macro-fracture effects are considered as part of an effective inorganic permeability. Thus, a compact form of the governing equations becomes as follows.

Free gas mass balance in the organic micropores (kerogen):

$$\phi_k\frac{\partial C_{ki}}{\partial t}+(1-\phi_k)\frac{\partial C_{\mu i}}{\partial t}=\frac{\partial}{\partial x}\left(\phi_k D_{ki}\frac{\partial C_{ki}}{\partial x}\right)+\frac{\partial}{\partial x}\left[(1-\phi_k)D_{si}\frac{\partial C_{\mu i}}{\partial x}\right]. \tag{10}$$

Free gas mass balance in inorganic matrix (macro-pores):

$$\phi_I\frac{\partial C_i}{\partial t}=\frac{\partial}{\partial x}\left[\phi_I Z_i RTC_i\frac{k}{\mu_i}\frac{\partial C_i}{\partial x}\right]-\Omega_m\Psi_{ki}(C_i-C_{ki}). \tag{11}$$

In Eq. (10) molecular diffusion D_{ki} is a measure of the micropore diffusion which may involve the bulk and/or Knudsen diffusion depending on the local shale gas conditions. Our previous experimental and numerical studies using Lattice Boltzmann method of gas dynamics simulation showed that the Knudsen diffusion is important only at the laboratory conditions where the pressure is below 200–500 psi, depending on the temperature and fluid composition (Fathi et al., 2012). In this study, we consider isothermal reservoir conditions with significantly high pressure values such that the kinetic effects of the pore wall–pore fluid interactions are suppressed and, hence, a simple micropore diffusion can be considered with a pore diffusivity for component i taken as a constant

$$D_{ki}=\frac{D_p}{q}=\frac{4\eta_0}{3\tau}\sqrt{\frac{8RT}{\pi M_i}}. \tag{12}$$

Here, η_0 is the Knudsen flow parameter and τ is the tortuosity factor. We note that the nature of diffusive transport in the organic micropores is different than those in the inorganic macropores and fractures. In the micropores, the gas molecules are in a physically adsorbed state and, hence, their binary transport is under the influence of the organic solid material which has different adsorption capacity for the components. In this case, the surface diffusivity D_{si} for the binary gas described in Eq. (10) has the diagonal and off-diagonal components of a second order diffusivity tensor D_{ii}:

$$D_{s1}=D_{11}+D_{12}\frac{\partial C_{\mu 2}/\partial x}{\partial C_{\mu 1}/\partial x} \tag{13a}$$

$$D_{s2} = D_{22} + D_{21}\frac{\partial C_{\mu 1}/\partial x}{\partial C_{\mu 2}/\partial x}. \tag{13b}$$

A detailed derivation of the surface diffusivity D_{si} is presented in Appendix A. Here, we note that the contribution of the off-diagonal term on the diffusivity of component i is dependent on the ratio of the concentration gradients of the adsorbed phase components. Hence, the mass flux of each component is related to the locally existing gradients of the binary system. The main- and cross-term diffusion coefficients are described as:

$$D_{ii} = \frac{C_{km} - C_{\mu j}}{C_{km} - C_{\mu i} - C_{\mu j}} D_{si0} + \alpha\left(D_{si0} D_{sj0}\right)^{1/2} \frac{\left(C_{\mu i} C_{\mu j}\right)^{1/2}}{C_{km} - C_{\mu i} - C_{\mu j}} \tag{14a}$$

$$D_{ij} = \frac{C_{\mu i}}{C_{km} - C_{\mu i} - C_{\mu j}} D_{si0} + \alpha\left(D_{si0} D_{sj0}\right)^{1/2} \left(\frac{C_{\mu i}}{C_{\mu j}}\right)^{1/2} \frac{C_{km} - C_{\mu i}}{C_{km} - C_{\mu i} - C_{\mu j}} \tag{14b}$$

where α is the lateral molecular interaction coefficient taking values in between $-1 \le \alpha \le 1$. In the case of co-diffusion, for example, when the direction of fluxes for CH_4 and CO_2 is the same, α takes positive values, i.e. production stages. As it can be seen from Eqs. (14a) and (14b), mass fluxes of the gas components in this case reach to a maximum when $\alpha = +1$; their values decrease with α and eventually reach to a minimum when $\alpha = 0$. In addition, $\alpha = +1$ corresponds to the case when there is no lateral interaction between the adsorbed molecules in the micro-pores, i.e., the extended Langmuir-type adsorption prevails; whereas, $\alpha = 0$ corresponds to the case when the lateral interaction reaches a maximum level. Thus, the lateral interaction in the adsorbed phase may decrease the fluxes and hence slow down the mass transport of the gas components from the organic micro-pores to the inorganic macro-pores. In our case, α will be calculated at each discrete time and location steps as described by Yang et al. (1991):

$$\alpha\left(C_{\mu 1}, C_{\mu 2}, \nabla C_{\mu 1}, \nabla C_{\mu 2}, C_{km}, D_{p1}, D_{p2}, D_{s10}, D_{s20}\right)$$

where C_m is defined as

$$\frac{1}{C_{km}} = \frac{c_{\mu 10}}{C_{\mu s1}} + \frac{c_{\mu 20}}{C_{\mu s2}} \tag{15a}$$

$$c_{\mu i0} = \frac{C_{\mu i0}}{C_{\mu 10} + C_{\mu 20}}; \quad i = 1, 2. \tag{15b}$$

Here, we consider that the binary gas mixture obeys the multi-component (extended-) Langmuir adsorption isotherm:

$$C_{\mu i} = \frac{C_{km} b_i' C_{ki}}{1 + b_1' C_{k1} + b_2' C_{k2}}; \quad i = 1, 2. \tag{16}$$

In general, the quantity $\Omega_m \Psi_{ki}$ has the dimensions of 1 / *time* and needs to be evaluated carefully. In the terminology of the conventional approach (diffusion-dominated matrix blocks with finite-size, R), an expression for it, which is dependent on the free and adsorbed gas concentrations, can be given as follows

$$\Omega_m \Psi_{ki} = \frac{15 D_{mi}}{R^2} = \frac{15}{R^2}\left[\varphi_k D_{ki} + (1-\varphi_k) D_{si}\left(\frac{C_{km} b_i' + C_{km} b_i' b_j' C_{kj}}{\left(1 + b_i' C_{ki} + b_j' C_{kj}\right)^2} - \frac{C_{km} b_i' b_j' C_{ki}}{\left(1 + b_i' C_{kj} + b_j' C_{kj}\right)^2} \frac{\partial C_{kj}}{\partial C_{ki}}\right)\right]. \tag{17}$$

These are the nature of the equations related to the CO_2 injection and enhanced shale gas production. Prior to setting up the initial/boundary value problems and numerically solving the governing Eqs. (10) and (11), the latter are written in the dimensionless form as follows:

(i) Dimensionless free CH_4 mass balance in organic micro-pores (kerogen):

$$\left(\delta_1 + \delta_2 g_1 - \delta_2 g_1' \frac{\partial c_{k2}}{\partial c_{k1}}\right) \frac{\partial c_{k1}}{\partial \tau} = \frac{\partial}{\partial r}\left[\left(1 + \varepsilon_1 g_1 - \varepsilon_1 g_1' \frac{\partial c_{k2}}{\partial c_{k1}}\right) \frac{\partial c_{k1}}{\partial r}\right] \tag{18a}$$

(ii) Dimensionless free CO_2 mass balance in organic micro-pores (kerogen):

$$\left(\delta_1 + \delta_2 g_2 - \delta_2 g_2' \frac{\partial c_{k1}}{\partial c_{k2}}\right) \frac{\partial c_{k2}}{\partial \tau} = \frac{\partial}{\partial r}\left[\left(1 + \varepsilon_2 g_2 - \varepsilon_2 g_2' \frac{\partial c_{k1}}{\partial c_{k2}}\right) \frac{\partial c_{k2}}{\partial r}\right] \tag{18b}$$

(iii) Dimensionless free CH_4 mass balance in inorganic matrix (macro-pores):

$$\delta_1 \frac{\partial c_1}{\partial \tau} = \frac{\partial}{\partial r}\left(\chi_1 c_1 \frac{\partial c_1}{\partial r}\right) - \gamma_1 (c_1 - c_{k1}) \tag{18c}$$

(iv) Dimensionless free CO_2 mass balance in inorganic matrix (macro-pores):

$$\delta_1 \frac{\partial c_2}{\partial \tau} = \frac{\partial}{\partial r}\left(\chi_2 c_2 \frac{\partial c_2}{\partial r}\right) - \gamma_2 (c_2 - c_{k2}). \tag{18d}$$

Details of scaling and non-dimensionalization are presented in Appendix B.

3. Initial/boundary value problem for CO_2 sequestration and enhanced shale gas recovery

The schematic of the problem is shown in Fig. 1. We consider the simulation of fluid dynamics in the matrix bounded by the two hydraulic fractures. For simplicity in the analysis, the problem can be reduced to a simpler one-dimensional form as shown in Fig. 2. Since we have multiple stages of operations during the CO_2 injection and enhanced shale gas recovery (including primary gas production, CO_2 injection, soaking, and secondary gas production) initial and boundary conditions relating to each stage need to be defined dynamically. Gas mixture is initially assumed to be 95.0% CH_4 and 5.0% CO_2, although these values can be changed relatively easily for another particular case study. Since

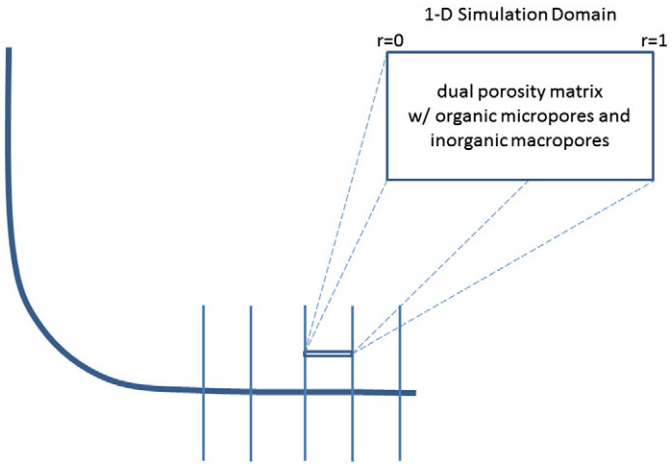

Fig. 1. Schematic of a cased and cemented horizontal well with a multi-stage hydraulically fractured lateral.

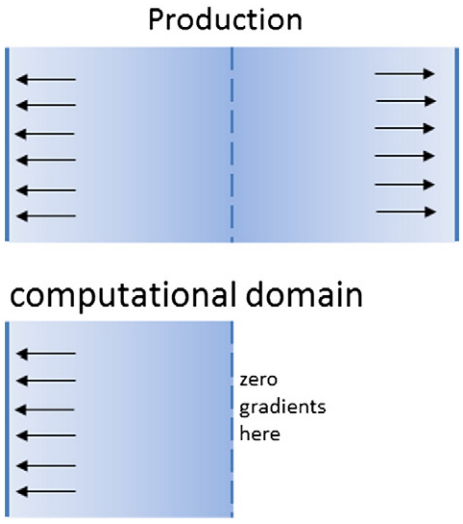

Fig. 2. Binary natural gas primary production operation for a single-well multiple-fracture setting.

organic materials are in micro- and meso-scales they are not intersected by the hydraulic fractures therefore the partial pressure of gas components at the left boundary is zero and partial pressure of gas components in inorganic materials is set to the commonly used bottom hole pressures in the dimensionless form. For the right hand side boundary we have no-flow boundary condition since we are simulating the half of the matrix block between two hydraulic fractures and we assume homogeneous and isotropic rock properties.

During the simulation of the first stage, i.e., CO_2 injection, and the third stage, i.e., secondary gas production, we use dynamic boundary conditions, i.e., the profiles at the end of previous stage become initial condition for the next stage. For the CO_2 injection rate we used mix boundary condition that relates the injection rate to mass flux in the reservoir, which is a more realistic approach in the field than assuming constant flow injection rate.

Initially we consider shale gas reservoir at 4660 psi pore pressure and the shale matrix contains a mixture of the components:

$$\tau = 0; \quad c_{k1}(r,0) = c_1(r,0) = 0.95; \quad c_{k2}(r,0) = c_2(r,0) = 0.05. \tag{19}$$

At the location of gas production, i.e., the hydraulic fracture face at the left boundary (Fig. 2), fixed concentration (partial pressure) conditions are specified for the components

$$r = 0; \quad c_{k1}(L,\tau) = c_{k2}(L,\tau) = 0; \quad c_1(L,\tau) = 0.05; \quad c_2(L,\tau) = 0.005. \tag{20}$$

On the other hand, at the center of the matrix block where the two hydraulic fractures interfere, we consider that CH_4 and CO_2 do not have any gradient. Hence, at the right boundary, we have:

$$r = 1; \quad \partial c_{k1}/\partial r = \partial c_1/\partial r = 0; \quad \partial c_{k2}/\partial r = \partial c_2/\partial r = 0 \tag{21}$$

The production stage lasts for 10 years and the concentrations (or partial pressures) at the end of the production stage have been used as initial condition for the next stage, i.e. CO_2 injection stage.

$$\tau = 0; \quad c_{k1}(r,0) = c_1(r,0) = 0.832; \quad c_{k2}(r,0) = c_2(r,0) = 0.168 \tag{22}$$

Since the horizontal well in the second stage is converted to CO_2 injection well, the boundary conditions are adjusted as follows.

At the location of CO_2 injection, i.e., the hydraulic fracture face at the left boundary (Fig. 3), fixed concentration condition is specified for CH_4; whereas the CO_2 gradient is inversely related to its flux in the reservoir J_{c2}:

$$r = 0; \quad c_{k1}(L,\tau) = c_1(L,\tau) = 0.832; \quad \partial c_{k2}/\partial r = \partial c_2/\partial r = -0.025/J_{c2}. \tag{23}$$

On the other hand, at the center of the matrix block between two hydraulic fractures, we consider that CH_4 and CO_2 do not have any gradient, right boundary:

$$r = 1; \quad \partial c_{k1}/\partial r = \partial c_1/\partial r = 0; \quad \partial c_{k2}/\partial r = \partial c_2/\partial r = 0. \tag{24}$$

CO_2 injection and soaking stage last for 5 years and gas concentrations (partial pressures) at the end of soaking have been used as initial condition for the secondary gas production stage, i.e., the third stage:

$$\tau = 0; \quad c_{k1}(r,0) = c_1(r,0) = 0.319; \quad c_{k2}(r,0) = c_2(r,0) = 0.681. \tag{25}$$

During the third stage the horizontal well is converted back to production well and the boundary conditions are adjusted as follows. At the location of gas production, i.e., the hydraulic fracture face at the left boundary (Fig. 3, bottom), fixed concentration (partial pressure) conditions are specified for the components:

$$r = 0; \quad c_{k1}(L,\tau) = c_{k2}(L,\tau) = 0; \quad c_1(L,\tau) = 0.05; \quad c_2(L,\tau) = 0.005. \tag{26}$$

On the other hand, at the center of the matrix block between two hydraulic fractures, we consider that CH_4 and CO_2 do not have any gradient, right boundary:

$$r = 1; \quad \partial c_{k1}/\partial r = \partial c_1/\partial r = 0; \quad \partial c_{k2}/\partial r = \partial c_2/\partial r = 0. \tag{27}$$

Eqs. (18a)–(18d) are coupled second order nonlinear partial differential equations, numerical approximation of which, with initial and boundary conditions specified in Eqs. (19)–(27), could be obtained using an implicit finite difference scheme and Newton iteration. Time integration of the ordinary differential equations resulting from the discretization in space is performed by a solver, which is based on an implicit linear multi-step method that chooses the time steps dynamically during the computations.

4. Results and discussion

We consider CO_2 sequestration and enhanced shale gas recovery using a unit of single horizontal well with multiple hydraulic fracturing stages in a shale gas reservoir with properties given in Table 1. At these conditions, the shale gas reservoir maintains an estimated 4660 psi of average initial reservoir pressure. 100 m spacing between uniform-sized hydraulic fractures is assumed. The simulation of CO_2 enhanced shale gas production continues for 45 years including 10 years of primary production followed by 5 years of CO_2 injection and 30 years of final production.

Fig. 1 shows the schematic of a cased and cemented horizontal well with a multi-stage hydraulically fractured lateral. It shows the one-dimensional computational domain with boundary conditions between two hydraulic fracture stages. Fig. 2 describes the binary natural gas production operation for a single-well multiple-fracture setting that is the first-stage in our CO_2 injection enhanced shale gas recovery operation. During the primary production CH_4 and CO_2 production rates are controlled by co-diffusive mass fluxes due to high pressure gradient near fracture face. After significant drop in initial reservoir pressure due to primary production, the second stage starts when the horizontal well is converted to CO_2 injection well. Fig. 3 depicts the CO_2 injection and CH_4 production operation for a single-well multiple-fracture setting where injection of CO_2 into organic-rich shale initiates counter-

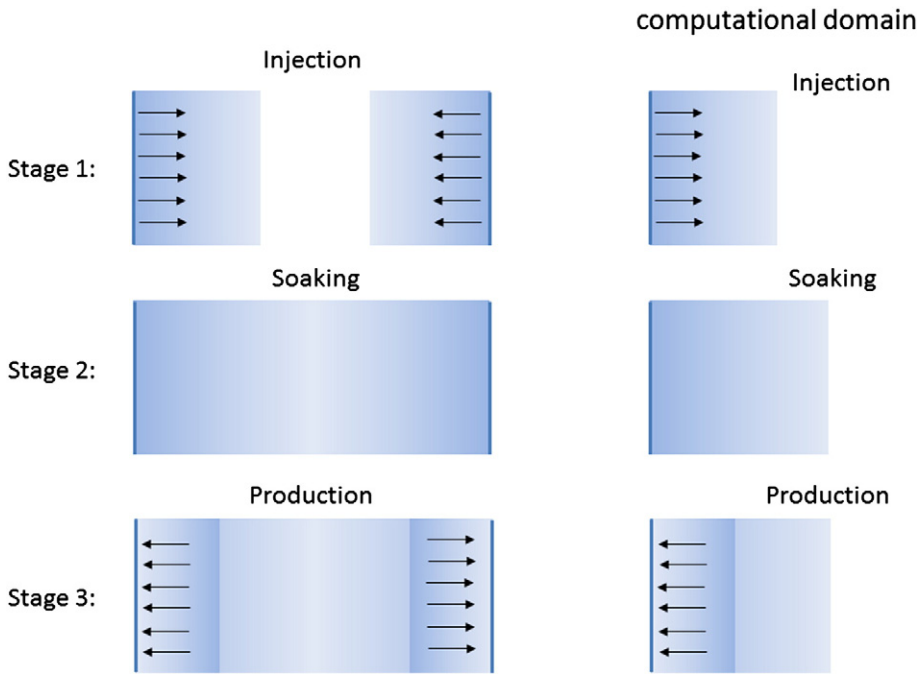

Fig. 3. CO_2 injection and CH_4 production as a three-stage operation for a single-well multiple-fracture setting.

diffusive transport and competitive (and often selective) sorption processes among the injected CO_2 and in place CH_4 gas molecules. Consequently, the incoming CO_2 molecules activate and displace the in-place CH_4 molecules. Competitive sorption rates, however, could be controlled by the counter-diffusive mass fluxes. After some period of CO_2 injection, the reservoir pressure builds up. Soaking period could last for several months to a year. After the reservoir system reaches to the new equilibrium conditions, the last stage of gas production begins and continues for the next 30 years when the average reservoir pressure approaches the bottom hole flowing pressure. The lateral molecular interaction coefficient α introduced earlier dictates in the reservoir where co- or counter-diffusive flux mechanism became dominated. As discussed earlier in our model α is a dynamic value and calculated at each location and time steps based on the definition by Yang et al. (1991).

Comparison of the methane production using a new model developed in this study with the conventional models is done first. Fig. 4A compares the two approaches in terms of the estimated total methane recoveries versus time. The difference between the models is due to the shale gas release kinetics approach and to the binary nature of the problem. Note that the quantity D_{si0} refers to surface diffusion in the absence of binary molecular interactions of the components and of their gradients. It is given as a constant $D_{s0} = D_{s10} = D_{s20}$ value. This value

Table 1
Base parameters used in primary CBM and CO_2-ECBM simulations.

Parameter	Unit	Value
ϕ_k	frac.	0.532%
ϕ_I	frac.	0.798%
ϕ	frac.	1.33%
k	nD	100
$C_{10} = C_{f10}$	mol/cm^3	3.8E−3
C_{20}–C_{f20}	mol/cm^3	2.0E−4
$C_{\mu s1}$	mol/cm^3	2.0E−3
$C_{\mu s2}$	mol/cm^3	3.0E−3
b_1	cm^3/mol	500.0
b_2	cm^3/mol	1200.0
$D_{k1} = D_{k2}$	cm^2/s	3.5E−5
$D_{s10}/D_{k1} = D_{s20}/D_{k2}$	–	1.0E−2
$D_{s20} = D_{s10}$	cm^2/s	1.1E−2
L	cm	1.0E4
T	K	322.04
R_g	kg cm^2/K/mol/s	8.314E4
μ	kg/cm/s	2.0E−7

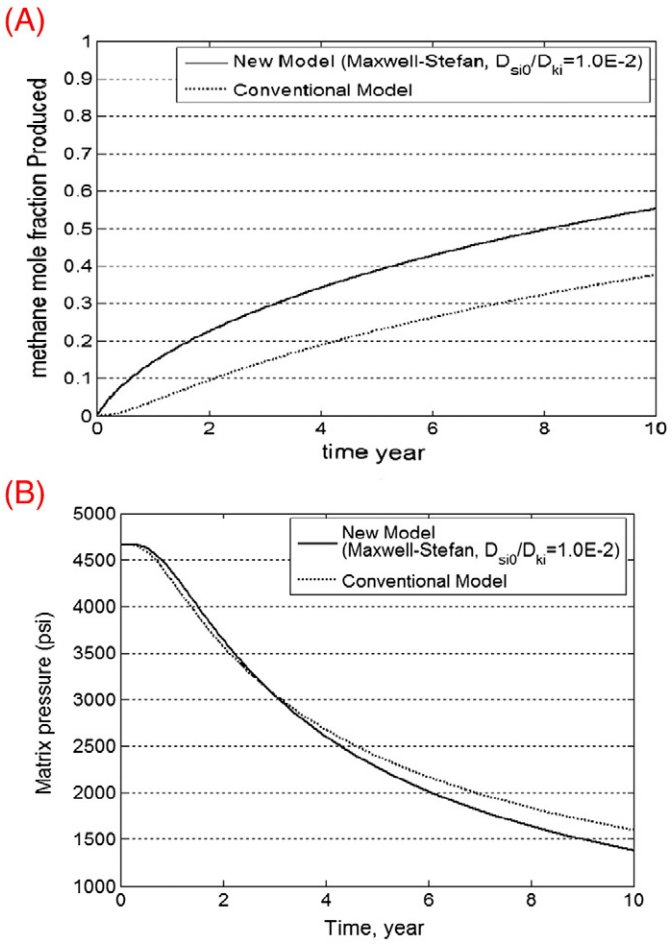

Fig. 4. Comparison of the Maxwell–Stefan model with the conventional model.

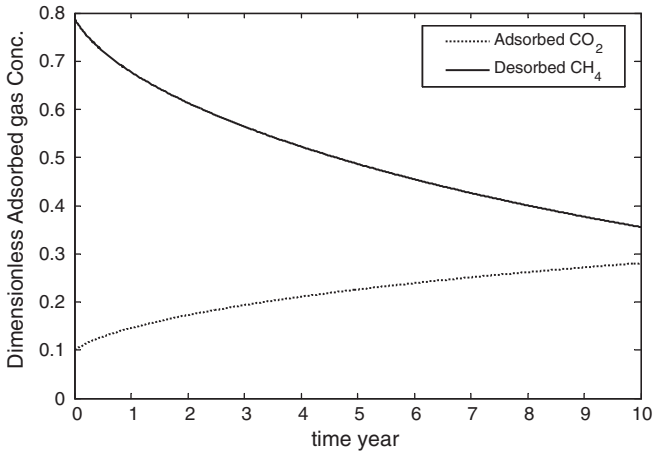

Fig. 5. Comparison between dimensionless CH_4 mole fraction replaced by CO_2 during primary gas production.

is different than D_{si} which is computed during the simulation using Eqs. (13a) and (13b). Application of the new formulation in primary gas production clearly shows the importance of the adsorbed phase transport, which leads to methane recovery up to 55% during the first 10 years while conventional model estimates only 20% recoveries. The additional recovery is 35% and indicating to us that the molecular phenomenon is likely to play an important and positive role during the production. Fig. 4B clearly illustrates that the new formulation has higher gas production rate that leads to significantly more pressure drop than the conventional model in shale gas reservoir pressure. After 10 years of primary gas production reservoir pressure drops from 4660 psi to 1388 psi when the second stage, i.e., CO_2 injection, starts. Fig. 5 illustrates the comparison between dimensionless CH_4 mole fraction replaced by CO_2 during the primary gas production. The strong selective sorption behavior leads to CO_2–CH_4 exchange in the organic micropores. This, in turn, increases the CO_2 adsorbed mole fraction significantly during the primary production and injection periods.

To start the CO_2 injection stage, gas concentrations (partial pressures) at the end of primary gas production used as initial conditions for the second stage, i.e., 83.0% CH_4 and 17.0% CO_2, and boundary conditions are modified as discussed earlier. CO_2 injection in shale gas reservoir lasts for 5 years. This leads to an increase in the reservoir pressure from 1388 psi to 3600 psi. Fig. 6 shows the pressure build up in the reservoir during the CO_2 sequestration period. Fig. 7 shows the comparison between CO_2 mole fraction sequestered and CH_4 desorbed during the

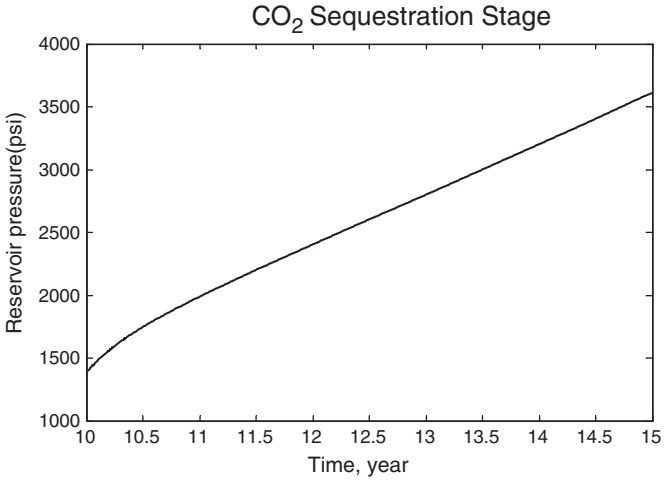

Fig. 6. Reservoir pressure builds up during CO_2 injection stage.

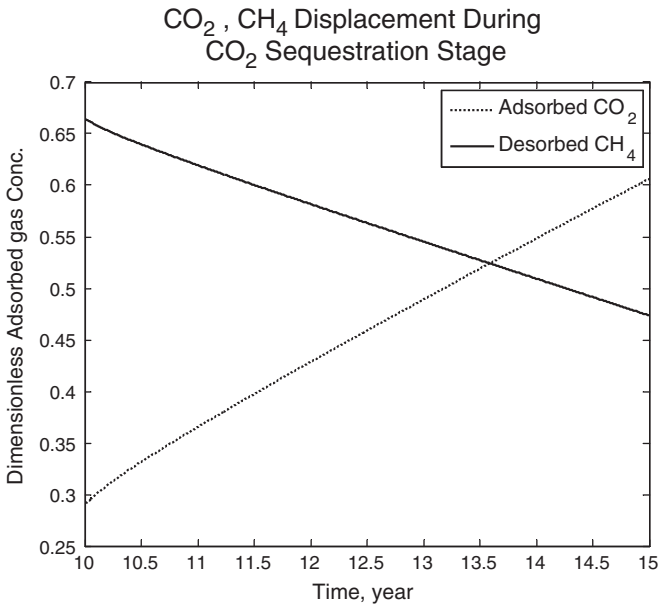

Fig. 7. Comparison between dimensionless CO_2 mole fraction injected and CH_4 produced.

CO_2-enhanced methane production process based on the Langmuir isotherms used in this study (see Table 1 for the Langmuir volume and the Langmuir pressure values). It also indicates that 2 CH_4 molecules are replaced by 3 CO_2 molecules. This is more than 1:1 exchange ratio. It

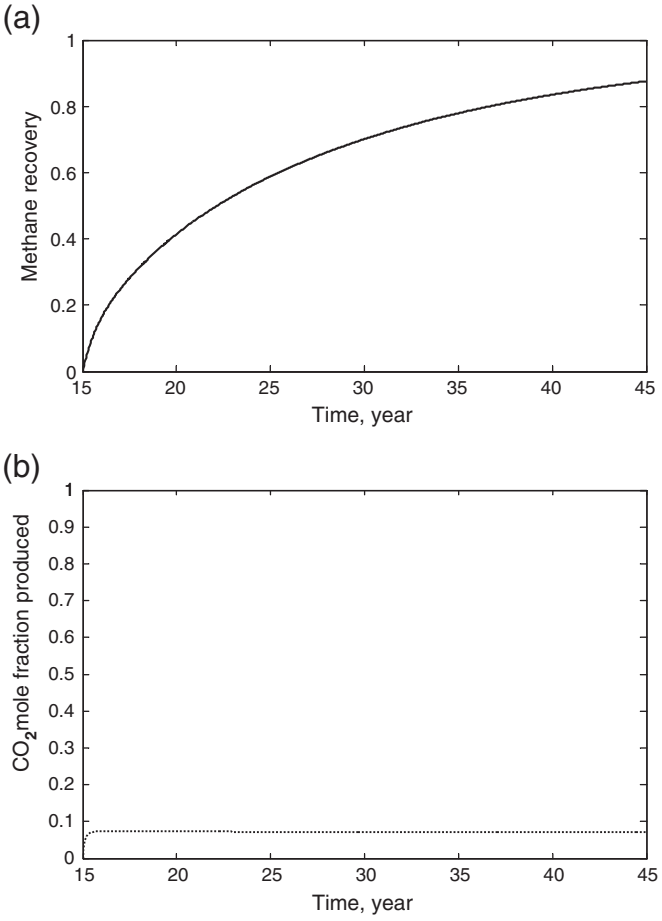

Fig. 8. (a): Enhanced methane recovery after CO_2 sequestration. (b): CO_2 mole fraction recovery during gas production after CO_2 sequestration.

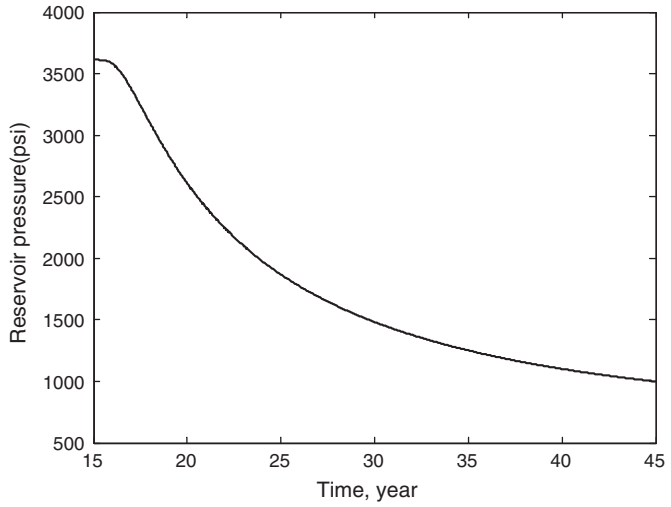

Fig. 9. Reservoir pressure decline after 30 years of production.

should be mentioned that this ratio could change based on shale gas total organic content (TOC) and the Langmuir isotherms used to describe gas sorption behavior. As it is clear from Fig. 7 the system has not reached to the maximum adsorption capacity since the adsorbed phase mole fraction has not reached to the plateau yet. Assuming the same rate of mass exchange between CO_2 and CH_4 gas molecules, the final equilibrium adsorbed and free gas concentration obtained are used as an initial condition for the last stage, i.e., the second stage of gas production.

Fig. 8a shows 30 years of methane recovery after CO_2 sequestration stage. Total gas recovery reaches to 85% of initial gas in place. Fig. 8b, however, shows that during the gas production stage only less than 10% of the injected CO_2 has been produced. It is clear that CO_2 injection is beneficial for methane recovery at every stage of methane production. This is due to the positive counter diffusion and competitive adsorption effects of the CO_2 molecule where small-scale steric effects cause significant change in a much larger field scale. Fig. 9 shows how the average reservoir pressure drops to constant bottom hole pressure during the production

5. Conclusions

Injection and storage of anthropogenic CO_2 in shale gas reservoirs have the benefit of producing additional methane which makes the injection and sequestration a low-cost procedure in these subsurface environments. Conventional numerical simulators, however, have limited predictive capabilities for the design and development of CO_2-enhanced shale gas recovery operation because they neglect certain physical mechanisms intrinsic to the technique and its application to the shale gas reservoirs. Focus of this paper was to develop a new triple-porosity single-permeability flow simulation model which is based on a new kinetic approach for the description of gas release from the organic micropores into the inorganic macropores and fractures. It is shown that the surface diffusion of the adsorbed molecules in the micropores is an important mechanism of transport during the CO_2-enhanced shale gas recovery since it leads to important counter diffusion and competitive adsorption effects. These small-scale effects have the potential to change the dynamics of injection and production operations at the field scale and they could be critical during the evaluation of commercial CO_2 injection projects.

Nomenclature

b	partition coefficient
b'	Langmuir isotherm constant [cm^3/mol]
c	dimensionless inorganic macro-pore free gas concentration
C	inorganic macro-pore free gas concentration [mol/cm^3 pore]
c_k	dimensionless organic micro-pore free gas concentration
C_k	organic micro-pore free gas concentration [mol/cm^3 pore]
c_μ	dimensionless adsorbed gas concentration
C_μ	adsorbed gas concentration [mol/cm^3 solid]
D_s	surface molecular diffusion coefficient [cm^2/s]
D_k	molecular pore diffusion coefficient [cm^2/s]
J	flux [cm^3/s]
k	matrix permeability [cm^2]
K_L	fracture dispersion coefficient [cm^2/s]
L	well spacing [cm]
M	molecular weight
r	dimensionless distance
R_g	universal gas constant
T	absolute temperature [K]
t	time coordinate [s]
x	space coordinate [cm]

Greek letters

α	lateral molecular interaction coefficient
ϕ_k	organic micro-pore porosity
ϕ_I	Inorganic macro-pore porosity
ϕ_I	fracture porosity
μ	gas viscosity [cp]
σ	matrix block shape factor [1/cm^2]
η_0	Knudsen flow parameter
ε_{kp}	kerogen pore volume per total matrix pore volume
ε_{ks}	total organic content (TOC) in terms of organic grain volume per total grain volume
Ψ	Diffusive transport
τ	dimensionless time

Subscript letters

0	related to initial amount
1	related to CH_4 component
2	related to CO_2 component
k	related to kerogen
m	related to matrix
f	related to fracture

Appendix A. Estimation of the surface diffusion coefficients, D_{s1} and D_{s2}

$$\frac{\partial C_{\mu 2}}{\partial x} = \frac{\partial}{\partial x}\left(\frac{C_{km} b_2' C_{k2}}{1 + b_1' C_{k1} + b_2' C_{k2}}\right) = \left[\frac{C_{km} b_2' + C_{km} b_1' b_2' C_{k1}}{(1 + b_1' C_{k1} + b_2' C_{k2})^2}\right]\frac{\partial C_{k2}}{\partial x} - \left[\frac{C_{km} b_1' b_2' C_{k2}}{(1 + b_1' C_{k1} + b_2' C_{k2})^2}\right]\frac{\partial C_{k1}}{\partial x} \quad (A-1)$$

$$\frac{\partial C_{\mu 1}/\partial x}{\partial C_{\mu 2}/\partial x} = \frac{(b_1' + b_1' b_2' C_{k2})\frac{\partial C_{k1}}{\partial x} - (b_1' b_2' C_{k1})\frac{\partial C_{k2}}{\partial x}}{(b_2' + b_1' b_2' C_{k1})\frac{\partial C_{k2}}{\partial x} - (b_1' b_2' C_{k2})\frac{\partial C_{k1}}{\partial x}} \quad (A-2)$$

$$D_{s1} = D_{11} + D_{12}\frac{(b_2' + b_1' b_2' C_{k1})\frac{\partial C_{k2}}{\partial x} - (b_1' b_2' C_{k2})\frac{\partial C_{k1}}{\partial x}}{(b_1' + b_1' b_2' C_{k2})\frac{\partial C_{k1}}{\partial x} - (b_1' b_2' C_{k1})\frac{\partial C_{k2}}{\partial x}}$$
$$D_{s2} = D_{22} + D_{21}\frac{(b_1' + b_1' b_2' C_{k2})\frac{\partial C_{k1}}{\partial x} - (b_1' b_2' C_{k1})\frac{\partial C_{k2}}{\partial x}}{(b_2' + b_1' b_2' C_{k1})\frac{\partial C_{k2}}{\partial x} - (b_1' b_2' C_{k2})\frac{\partial C_{k1}}{\partial x}} \quad (A-3)$$

Appendix B. Scaling and non-dimensionalization

$$c_{k1}=\frac{C_{k1}}{C_{k10}+C_{k20}},c_{k2}=\frac{C_{k2}}{C_{k10}+C_{k20}},c_{\mu 1}=\frac{C_{\mu 1}}{C_{\mu 10}+C_{\mu 20}},$$
$$c_1=\frac{C_1}{C_{k10}+C_{k20}},c_2=\frac{C_2}{C_{k10}+C_{k20}}$$
$$c_{\mu 2}=\frac{C_{\mu 2}}{C_{\mu 10}+C_{\mu 20}},c_{km}=\frac{C_{km}}{C_{\mu 10}+C_{\mu 20}},r=\frac{x}{L},\tau=\frac{\delta_1 D_{k1}t}{L^2}=\frac{\delta_1 D_{k2}t}{L^2}$$

$$\delta_1=\frac{1}{1+\left(\frac{1-\phi_k}{\phi_k}\right)\left(\frac{C_{\mu 10}+C_{\mu 20}}{C_{k10}+C_{k20}}\right)},\quad \delta_2=1-\delta_1 \tag{B-1}$$

$$\begin{aligned}\varepsilon_1&=\left(\frac{C_{\mu 10}+C_{\mu 20}}{C_{k10}+C_{k20}}\right)\left(\frac{1-\phi_k}{\phi_k}\right)\left(\frac{D_{s1}}{D_{s10}}\right)\left(\frac{D_{s10}}{D_{k1}}\right)\\ \varepsilon_2&=\left(\frac{C_{\mu 10}+C_{\mu 20}}{C_{k10}+C_{k20}}\right)\left(\frac{1-\phi_k}{\phi_k}\right)\left(\frac{D_{s2}}{D_{s20}}\right)\left(\frac{D_{s20}}{D_{k2}}\right)\end{aligned} \tag{B-2}$$

$$\delta_1\frac{\partial c_{ki}}{\partial\tau}+\delta_2\frac{\partial c_{\mu i}}{\partial\tau}=\frac{\partial}{\partial r}\left(\frac{\partial c_{ki}}{\partial r}\right)+\frac{\partial}{\partial r}\left(\varepsilon_i\frac{\partial c_{\mu i}}{\partial r}\right);\qquad i=1,2 \tag{B-3}$$

$$c_{\mu i}=\frac{c_{km}\lambda_i c_{ki}}{1+\lambda_1 c_{k1}+\lambda_2 c_{k2}};\qquad i=1,2 \tag{B-4}$$

$$\lambda_1=b_1'(C_{k10}+C_{k20}),\qquad \lambda_2=b_2'(C_{k10}+C_{k20}) \tag{B-5}$$

$$\begin{aligned}\frac{\partial c_{\mu 1}}{\partial\tau}&=g_1\frac{\partial c_{k1}}{\partial\tau}-g_1'\frac{\partial c_{k2}}{\partial\tau}\\ \frac{\partial c_{\mu 2}}{\partial\tau}&=g_2\frac{\partial c_{k2}}{\partial\tau}-g_2'\frac{\partial c_{k1}}{\partial\tau}\end{aligned} \tag{B-6}$$

$$\begin{aligned}g_1(c_{k1},c_{k2})&=\frac{c_{km}\lambda_1(1+\lambda_2 c_{k2})}{(1+\lambda_1 c_{k1}+\lambda_2 c_{k2})^2}\\ g_2(c_{k1},c_{k2})&=\frac{c_{km}\lambda_2(1+\lambda_1 c_{k1})}{(1+\lambda_1 c_{k1}+\lambda_{k2} c_{k2})^2}\end{aligned} \tag{B-7}$$

$$\begin{aligned}g_1'(c_{k1},c_{k2})&=\frac{c_m\lambda_1\lambda_2 c_{k1}}{(1+\lambda_1 c_{k1}+\lambda_2 c_{k2})^2}\\ g_2'(c_{k1},c_{k2})&=\frac{c_m\lambda_1\lambda_2 c_{k2}}{(1+\lambda_1 c_{k1}+\lambda_2 c_{k2})^2}\end{aligned} \tag{B-8}$$

$$\frac{\partial}{\partial r}\left(\varepsilon_1\frac{\partial c_{\mu 1}}{\partial r}\right)=\frac{\partial}{\partial r}\left(\varepsilon_1 g_1\frac{\partial c_{k1}}{\partial r}\right)-\frac{\partial}{\partial r}\left(\varepsilon_1 g_1'\frac{\partial c_{k2}}{\partial r}\right) \tag{B-9}$$

$$\frac{\partial}{\partial r}\left(\varepsilon_2\frac{\partial c_{\mu 2}}{\partial r}\right)=\frac{\partial}{\partial r}\left(\varepsilon_2 g_2\frac{\partial c_{k2}}{\partial r}\right)-\frac{\partial}{\partial r}\left(\varepsilon_2 g_2'\frac{\partial c_{k1}}{\partial r}\right) \tag{B-10}$$

$$(\delta_1+\delta_2 g_1)\frac{\partial c_{k1}}{\partial\tau}-(\delta_2 g_1')\frac{\partial c_{k2}}{\partial\tau}=\frac{\partial}{\partial r}\left[(1+\varepsilon_1 g_1)\frac{\partial c_{k1}}{\partial r}\right]-\frac{\partial}{\partial r}\left(\varepsilon_1 g_1'\frac{\partial c_{k2}}{\partial r}\right) \tag{B-11}$$

$$(\delta_1+\delta_2 g_2)\frac{\partial c_{k2}}{\partial\tau}-(\delta_2 g_2')\frac{\partial c_{k1}}{\partial\tau}=\frac{\partial}{\partial r}\left[(1+\varepsilon_2 g_2)\frac{\partial c_{k2}}{\partial r}\right]-\frac{\partial}{\partial r}\left(\varepsilon_2 g_2'\frac{\partial c_{k1}}{\partial r}\right) \tag{B-12}$$

which could be further simplified into

$$\left(\delta_1+\delta_2 g_1-\delta_2 g_1'\frac{\partial c_{k2}}{\partial c_{k1}}\right)\frac{\partial c_{k1}}{\partial\tau}=\frac{\partial}{\partial r}\left[\left(1+\varepsilon_1 g_1-\varepsilon_1 g_1'\frac{\partial c_{k2}}{\partial c_{k1}}\right)\frac{\partial c_{k1}}{\partial r}\right] \tag{18a}$$

$$\left(\delta_1+\delta_2 g_2-\delta_2 g_2'\frac{\partial c_{k1}}{\partial c_{k2}}\right)\frac{\partial c_{k2}}{\partial\tau}=\frac{\partial}{\partial r}\left[\left(1+\varepsilon_2 g_2-\varepsilon_2 g_2'\frac{\partial c_{k1}}{\partial c_{k2}}\right)\frac{\partial c_{k2}}{\partial r}\right] \tag{18b}$$

$$\begin{aligned}\frac{D_{11}}{D_{s10}}&=(1+\lambda_1 c_{k1})+\alpha\left(\frac{D_{s20}}{D_{s10}}\right)^{1/2}(\lambda_2\lambda_1 c_{k2}c_{k1})^{1/2}\\ \frac{D_{22}}{D_{s20}}&=(1+\lambda_2 c_{k2})+\alpha\left(\frac{D_{s10}}{D_{s20}}\right)^{1/2}(\lambda_2\lambda_1 c_{k2}c_{k1})^{1/2}\end{aligned} \tag{B-13}$$

$$\begin{aligned}\frac{D_{12}}{D_{s10}}&=\lambda_1 c_{k1}+\alpha\left(\frac{D_{s20}}{D_{s10}}\right)^{1/2}\left(\frac{\lambda_1 c_{k1}}{\lambda_2 c_{k2}}\right)^{1/2}(1+\lambda_2 c_{k2})\\ \frac{D_{21}}{D_{s20}}&=\lambda_2 c_{k2}+\alpha\left(\frac{D_{s10}}{D_{s20}}\right)^{1/2}\left(\frac{\lambda_2 c_{k2}}{\lambda_1 c_{k1}}\right)^{1/2}(1+\lambda_1 c_{k1})\end{aligned} \tag{B-14}$$

and in the inorganic macropores we have

$$\gamma_1=\frac{\Omega\Psi_{k1}L^2}{\phi_I D_{k1}},\chi_1=\left(\frac{(C_{k10}+C_{k20})}{D_{k1}}\right)\left(\frac{z_1 R_g T k}{\mu_1}\right) \tag{B-15}$$

$$\gamma_2=\frac{\Omega\Psi_{k2}L^2}{\phi_I D_{k2}},\chi_2=\left(\frac{(C_{k10}+C_{k20})}{D_{k2}}\right)\left(\frac{z_2 R_g T k_f}{\mu_2}\right) \tag{B-16}$$

$$\delta_1\frac{\partial c_i}{\partial\tau}=\frac{\partial}{\partial r}\left(\chi_i c_i\frac{\partial c_i}{\partial r}\right)-\gamma_i(c_i-c_{ki});\qquad i=1,2 \tag{18c}$$

$$\delta_1\frac{\partial c_2}{\partial\tau}=\frac{\partial}{\partial r}\left(\chi_2 c_2\frac{\partial c_2}{\partial r}\right)-\gamma_2(c_2-c_{k2}) \tag{18d}$$

References

Akkutlu, I.Y., Fathi, E., 2012. Multiscale gas transport in shales with local Kerogen heterogeneities. SPE Journal 17 (4).

Bear, J., Bachmat, Y., 1991. Introduction to Modeling of Transport Phenomena in Porous Media. Kluwer Academic Publishers, Dordrecht.

Bear, J., 1972. Dynamics of Fluids in Porous Media. American Elsevier, New York.

Boswell, R., 1996. Play UDs: upper Devonian black shales. The Atlas of Major Appalachian Gas Plays. Morgantown, WV, West Virginia Geological and Economic Survey, Publication, vol. 25, pp. 93–99.

Busch, A., Alles, S., Gensterblum, Y., Prinz, D., Dewhurst, D.N., Raven, M.D., Stanjek, H., Krooss, B.M., 2008. Carbon dioxide storage potential of shales. International Journal of Greenhouse Gas Control 2 (3), 297–308.

Chen, Z., Liu, J., Elsworth, D., Connell, L.D., Pan, Z., 2010. Impact of CO_2 injection and differential deformation on CO_2 injectivity under in-situ stress conditions. International Journal of Coal Geology 81 (2), 97–108.

Eccles, J.K., Pratson, L., Newell, R.G., Jackson, R.B., 2009. Physical and economic potential of geological CO_2 storage in saline aquifers. Environmental Science and Technology 43.

Fathi, E., Akkutlu, I.Y., 2013. Lattice Boltzmann method for simulation of shale gas transport in kerogen. SPE Journal 18 (1).

Fathi, E., Tinni, O., Akkutlu, I.Y., 2012. Correction to Klinkenberg slip theory for gas dynamics in nano-capillaries. International Journal of Coal Geology 103, 51–59.

Fathi, E., Akkutlu, I.Y., 2012. Mass transport of adsorbed-phase in stochastic porous medium with fluctuating porosity field and nonlinear gas adsorption kinetics. Journal of Transport in Porous Media 91 (1), 5–33.

Fathi, E., Akkutlu, I.Y., 2009. Matrix heterogeneity effects on gas transport and adsorption in coalbed and shale gas reservoirs. Journal of Transport in Porous Media 80 (2), 281–304.

Gwo, J., O'Brien, R., Jardin, P., 1998. Mass transfer in structured porous media: embedding meso-scale structure and microscale hydrodynamics in a two-region model. Journal of Hydrology 208, 204–222.

Kang, S.M., Fathi, E., Ambrose, R.J., Akkutlu, I.Y., Sigal, R.F., 2011. Carbon dioxide storage capacity of organic-rich shales. SPE Journal 16 (4), 842–855.

Leahy-Dios, A., Das, M., Agarwal, A., Kaminsky, R.D., 2011. Modeling of transport phenomena and multicomponent sorption for shale gas and coalbed methane in an unstructured grid simulator. SPE 147352-MS.

Nuttall, K.E., Rushing, J.A., 2005. Analysis of Devonian black shales in Kentucky for potential carbon dioxide sequestration and enhanced natural gas recovery. Kentucky Geological Survey Report DE-FC26-02NT41442.

Ryan, E.M., Tartakovsky, A.M., Amon, C., 2011. Pore-scale modeling of competitive adsorption in porous media. Journal of Contaminant Hydrology 120–121, 56–78.

Santos, J.M.R., Akkutlu, I.Y., 2013. Laboratory measurement of sorption isotherm under confining stress with pore volume effects. SPE 162595-MS.

Sarma, P., Aziz, K., 2006. New Transfer Functions for Simulation of Naturally Fractured Reservoirs with Dual Porosity Models. SPE 90231.Soc. of Pet. Eng., Dallas, Texas.

Schepers, K.C., Nuttall, B.C., Oudinot, A.Y., Gonzalez, R., 2009. Reservoir modeling and simulation of the Devonian gas shale of eastern Kentucky for enhanced gas recovery and CO_2 storage. SPE 126620-PP.Society of Petroleum Engineers.

Shi, J.Q., Durucan, S., 2008. Modeling of mixed-gas adsorption and diffusion in coalbed reservoirs. SPE 114197.Soc. of Pet. Eng., Dallas, Texas.

Shi, J.Q., Durucan, S., 2005. Gas storage and flow in coalbed reservoirs: implementation of a bidisperse pore model for gas diffusion in a coal matrix. SPE Reservoir Evaluation & Engineering 8 (2).

Tinni, A., Fathi, E., Agrawal, R., Sondergeld, C., Akkutlu, I.Y., Rai, C., 2012. Shale permeability measurements on plugs and crushed samples. SPE-162235.

Warren, J.E., Root, P.J., 1963. The behaviour of naturally fractured reservoirs. SPE Journal 3 (11), 245–255.

Yang, R.T., Chen, Y.D., Yeh, Y.T., 1991. Prediction of cross-term coefficients in binary diffusion: diffusion in zeolite. Chemical Engineering Science 46 (12), 3089–3099.

Yi, J., Akkutlu, I.Y., Deutsch, C.V., 2008. Gas transport in bidisperse coal particles: investigation for an effective diffusion coefficient in coalbeds. Journal of Canadian Petroleum Technology 47 (10).

Zhou, L., Feng, Q., Chen, Z., Liu, J., 2012. Modeling and upscaling of binary gas coal interactions in CO_2 enhanced coalbed methane recovery. Procedia Environmental Sciences 12 (Part B), 926–939.